

See discussions, stats, and author profiles for this publication at: <https://www.researchgate.net/publication/231654393>

Nanosheet-Based NiO Microspheres: Controlled Solvothermal Synthesis and Lithium Storage Performances

ARTICLE *in* THE JOURNAL OF PHYSICAL CHEMISTRY C · DECEMBER 2009

Impact Factor: 4.77 · DOI: 10.1021/jp909014w

CITATIONS

141

READS

54

7 AUTHORS, INCLUDING:



Manman Ren

Qilu University of Technology

10 PUBLICATIONS 578 CITATIONS

[SEE PROFILE](#)



Chunsheng Sun

Jiangnan University

2 PUBLICATIONS 140 CITATIONS

[SEE PROFILE](#)



Zhen Zhou

Nankai University

211 PUBLICATIONS 6,680 CITATIONS

[SEE PROFILE](#)

Nanosheet-Based NiO Microspheres: Controlled Solvothermal Synthesis and Lithium Storage Performances

Lu Liu,* Yue Li, Shuming Yuan, Ming Ge, Manman Ren, Chunsheng Sun, and Zhen Zhou*

Tianjin Key Laboratory of Environmental Remediation and Pollution Control and Institute of New Energy Material Chemistry, Nankai University, Tianjin 300071, People's Republic of China

Received: September 17, 2009; Revised Manuscript Received: November 23, 2009

Two-dimensional (2D) nanosheets directly grew into three-dimensional (3D) microspheres through a one-step solvothermal route under controlled conditions; during this procedure the decomposition of hexamethylenetetramine at temperatures higher than 120 °C provided OH⁻ at the rate of good diffusion, and surfactants were used as templates to provide the growth sites and control the crystalline growth direction. By means of the Ostwald ripening process, precursor microspheres formed with narrowly distributed diameters, and then NiO 3D microspheres were obtained with further calcination at 300 °C for 2 h. NiO microspheres presented a high initial discharge capacity as anode materials in Li ion batteries, but degraded quickly during subsequent cycles, and further improvement in cyclic stability is still needed for practical application in Li ion batteries.

1. Introduction

In recent years, the synthesis of inorganic nanomaterials with controllable hierarchical structures has been attracting much interest.^{1,2} Nanostructured materials with complex morphologies analogous to biominerals,³ especially curved three-dimensional (3D) microspheres, exhibit promising applications in catalysis, Li ion batteries, water treatment, wettability, etc.^{4–7} Therefore, the synthesis of 3D microspheres is becoming an emerging subfield in both biomimetic synthesis and nanosciences. Metal,^{4–6} metal oxide,^{7–17} and sulfide^{4–6,18} 3D microspheres with solid or hollow interiors have been prepared. However, the precise morphology control of 3D microspheres with 2D nanosheet assembly is still a big challenge.

Nickel oxide (NiO) is an antiferromagnetic semiconductor with a wide band gap of ~3.6 eV¹⁹ and is used in various fields, such as catalysis,²⁰ electrochromic films,²¹ fuel cell electrodes,²² and active optical fibers.²³ At present, synthesis of nanostructured NiO in various forms, including nanoparticles,²⁴ nanowires,²⁵ nanorods,²⁶ nanosheets,²⁷ nanorolls,²⁸ hollow spheres,²⁹ and porous solids,³⁰ has widely been reported in recent years. Thermal decomposition of nitrates,²⁴ template-assisted carbothermal method,³¹ hydrothermal method,²⁹ etc., have been adopted for synthesis of nanostructured NiO.

Since Poizot et al.³² reported that nanosized transition-metal oxides (M_xO_y, where M is Ni, Fe, Co, or Cu) can act as anode materials for Li ion batteries, nanostructured oxides including NiO have been exploited as Li ion battery materials^{33–37} for the higher electrochemical capacity than that of the commercial graphite anode material (372 mA h/g). The reaction of NiO with Li is not an intercalation but a conversion process: NiO + 2Li⁺ → Li₂O + Ni - 2e. This leads to the formation of metallic Ni and Li₂O nanoparticles accompanied with large volume expansion. When NiO is used as the anode material for Li ion batteries, its theoretical capacity is about 718 mA h/g. However, the large volume expansion/constriction can lead to the pulverization and degradation of the electrodes, resulting in serious

capacity degradation and poor cycling performance. One method to alleviate the problem is to prepare materials with small particles. It has recently been reported that NiO nanowalls show excellent capacity retention and high rate performance during cycling.^{38,39}

Herein, we report the synthesis of NiO with microsphere-like morphologies through solvothermal route and subsequent calcination. The decomposition of hexamethylenetetramine at temperatures ≥120 °C provided OH⁻ at the rate of good diffusion, and surfactants were used as templates. Using a similar synthetic strategy, we have synthesized Fe₂O₃ nanorods and nanotubes,⁴⁰ TiO₂,⁴¹ ZnO,⁴² and In₂S₃⁴³ microspheres. The present work suggests that it is possible to grow directly 2D nanosheets into 3D microspheres through a one-step solvothermal route under controlled conditions and then to obtain metal oxide 3D microspheres with further calcination at appropriate temperatures.

2. Experimental Section

2.1. Synthetic Process of NiO 3D Microspheres. A 0.3 g amount of NiCl₂ and 0.4 g of hexamethylenetetramine were put into a Teflon-lined stainless steel autoclave of 50 mL capacity, and then the autoclave was filled with 15 mL of distilled water and 0.4 g of sodium dodecyl sulfate (SDS) as well as 15 mL of butanol. After the autoclave was maintained at 150 °C for 24 h without shaking or stirring during the heating period, it was cooled to room temperature naturally. A black precipitate was collected and then washed with distilled water and absolute ethanol to remove surfactant and organic impurities. Finally the precipitate was calcined at 300 °C for 2 h and then was kept in absolute ethanol.

2.2. Sample Characterization. X-ray diffraction analysis of the samples was carried out under X-ray diffractometer (XRD, D/MAX2500, Rigaku) with Cu K α radiation ($\lambda = 1.54056 \text{ \AA}$). The morphology of the as-prepared products was characterized with scanning electron microscopy (SEM, Hitachi-530, SEM/EDX JEOL JSM-6700F) and transmission electron microscopy (TEM, JEOL-2010, operating voltage of 200 kV), high-resolution TEM (HRTEM, JEOL-2010), and X-ray photoelectron spectroscopy (XPS, Kratos Axis Ultra DLD).

* To whom correspondence should be addressed. Tel.: +86-22-23504015. Fax: +86-22-23498941. E-mail: liul@nankai.edu.cn (L.L.); zhouchen@nankai.edu.cn (Z.Z.).

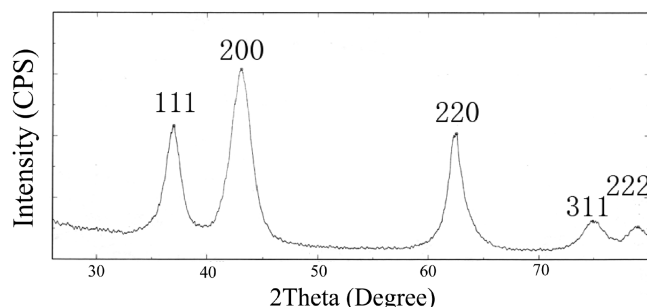


Figure 1. XRD pattern of NiO microspheres.

2.3. Electrochemical Tests. Electrochemical Li storage performances of the samples were evaluated in Li test cells. The anode electrodes were prepared by mixing the samples with acetylene black and poly(tetrafluoroethylene) (PTFE) with a weight ratio of 75:20:5 in ethanol to ensure homogeneity. After the ethanol was evaporated, the mixture was rolled into a sheet, and the sheet was cut into circular strips of 8 mm in diameter. The strips were then dried at 100 °C for 10 h. Lithium metal was used as the reference and counter electrode. The electrolyte was composed of a 1 mol L⁻¹ LiPF₆ dissolved in ethylene carbonate/dimethyl carbonate/ethylene methyl carbonate (EC/DMC/EMC) with the volume ratio of 1:1:1. Test cells were assembled in an argon-filled dry glovebox. The galvanostatic charge/discharge tests were performed with a Land CT2001 battery tester. The current density was 50 mA/g in a potential range of 0.01–3.0 V at 25 °C.

3. Results and Discussion

3.1. Preparation and Characterization of NiO 3D Microspheres. Figure 1 shows XRD patterns of the as-prepared microspheres. It can be seen that the XRD pattern conforms with the face-centered cubic (fcc) ($a = 4.177 \text{ \AA}$, JCPDS file No. 47-1049), and no characteristic peaks are observed for other impurities such as NiCO₃ and Ni. All peaks can be assigned to the diffraction from the (111), (200), (220), (311), and (222) planes of the cubic NiO, respectively. This indicates that pure crystalline NiO formed via the solvothermal and calcination process. From Figure 1, it can also be seen that the relative diffraction intensity of (220) and (200) is higher than the corresponding conventional value (JCPDS file No. 71-1179). This observation indicates that the resultant NiO nanosheets are mainly dominated by (200) and (220) facets. The XPS spectra of the microspheres for the O_{1s} and Ni_{2p} core levels are shown in Figure S1 (Supporting Information). The binding energies of the main and satellite peaks in the O_{1s} and Ni_{2p} core levels are consistent with the previous report on NiO.¹⁷

Low-magnification SEM images show that the as-obtained NiO samples are composed of many uniform, spherelike architectures ranging from 2 to 6 μm in diameter (Figure 2a). Higher magnification SEM images reveal that NiO microspheres are built from small-crystal 2D nanosheets with thickness of 20 nm. These crystal thin sheets, analogous to a chrysanthemum, are aligned to the spherical surface, pointing toward a common center (Figure 2b,c).

Figure 3a shows a few typical TEM images of the NiO nanosheet-based spherelike structure. Figure 3b shows a typical TEM image of an isolated NiO nanosheet-based spherelike structure. The edge portion of the spherelike structure is lighter than that of the center and is comprised of sheetlike 2D nanostructures. The HRTEM image of a single nanosheet in the microspheres shows the single-crystalline structure (Figure

3c). The lattice spacing of 0.209 nm corresponds to the d spacing between adjacent (200) crystallographic planes of NiO nanosheets. The as-synthesized nanosheets are elongated along the (200) and (220) direction; the long axis of the nanosheets is parallel to the [200] direction.

3.2. Effects of Synthetic Conditions on NiO Morphologies.

The relationship between NiO shapes and synthetic time was also investigated. The synthetic times were 0.5, 1, 2, 4, 8, and 24 h, respectively, and the SEM images are shown in Figure 4a–e and Figure 2. Irregular shapes consisted of sheets formed for the synthetic time of 0.5 h (Figure 4a), many spherelike shapes formed for the synthetic time of 1 h (Figure 4b), and clear nanosheet morphology appeared for the synthetic time of 2 h (Figure 4c). As the reaction time increased, clearer nanosheet morphology formed (Figure 4d,e), and nanosheet-based microspheres with narrowly distributed diameters were obtained for the reaction time of 24 h, as shown in Figure 2. The results reveal that reaction time is the main factor to form nanosheet-based NiO microspheres with narrowly distributed diameters; that is, the Ostwald ripening process is indispensable.

We also investigated the effect of calcination temperature on the morphology of NiO. When the precursor was calcined in air at 300 °C for 2 h, NiO microspheres were obtained, as shown in Figure 5a; when the precursor was calcined in air at 400 °C for 2 h, NiO nanosheets with a thickness of 10 nm were obtained, as shown in Figure 5b; when the calcination temperature was increased to 600 °C, NiO with irregular morphologies formed, as shown in Figure 5c, which reveals that appropriate temperature is indispensable in keeping the shapes of precursor microspheres during the calcination process.

Several experiments were also carried out to determine the roles of the solvents and surfactants in the formation of NiO microspheres. Only NiO nanosheets were produced, if *n*-butanol is replaced by *n*-octanol (Figure 6a). The use of surfactant Span80 as templates resulted in irregular NiO microspheres (Figure 6b). When H₂O and butanol were used as solvent and no surfactant SDS was added, irregular NiO microspheres were produced (Figure 6c). With water as solvent and the absence of SDS, only nanosheets were obtained (Figure 6d). Only under the condition that water was used as solvent and the surfactant SDS was present in the system were NiO microspheres with diameters of 50 nm produced, as shown in Figure 6e.

On the basis of the above results, we can propose a growth process of the 3D microspheres with NiO 2D nanosheet assembly. It is known that the higher the ratio of surface atoms is, the stronger the XRD peak is. When the surfactant is used, the surfactant molecules can cap on the crystal surface selectively. Generally, the face with a higher density of surface atoms is blocked by the adsorption of surfactants during the crystal growth of colloidal nanocrystals, and the growth along this facet is therefore considerably restricted.⁴⁴ In the synthetic process, the growth is inhibited in the direction perpendicular to the (201) precursor (Ni₂CO₃(OH)₂) crystal surface, resulting in flexible nanosheets that could readily intermesh with each other to form a 3D porous structure.⁴⁵ Herein, it is emphasized that the surfactants are indispensable for 2D nanosheets to form 3D microspheres. Without any surfactant, the chrysanthemum-like 3D microspheres do not form. There are C=O, S=O, -O⁻, and SO₃²⁻ functional groups in surfactant molecules, which provide coordination sites for cations.⁴⁶ Before the synthetic reaction occurs, a lot of Ni²⁺ ions gather on coordination sites. Over 120 °C, hexamethylenetetramine decomposes to release OH⁻ and CO₃²⁻, and forms a Ni₂CO₃(OH)₂ crystal nucleus. Then, these instantaneously produced Ni₂CO₃(OH)₂ nanoclusters in

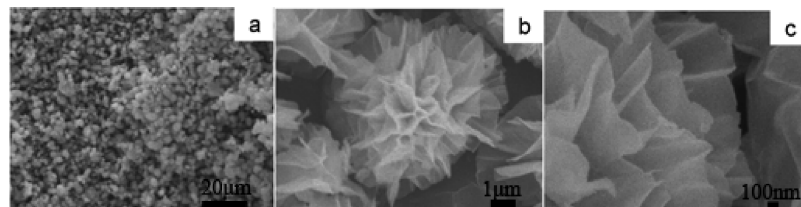


Figure 2. SEM images of NiO microspheres with low magnification (a), medium magnification (b), and high magnification (c).

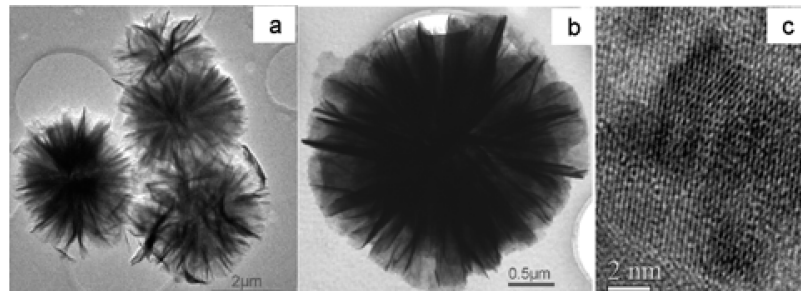


Figure 3. TEM images of NiO microspheres: (a) Low magnification, (b) high magnification, and (c) HRTEM.

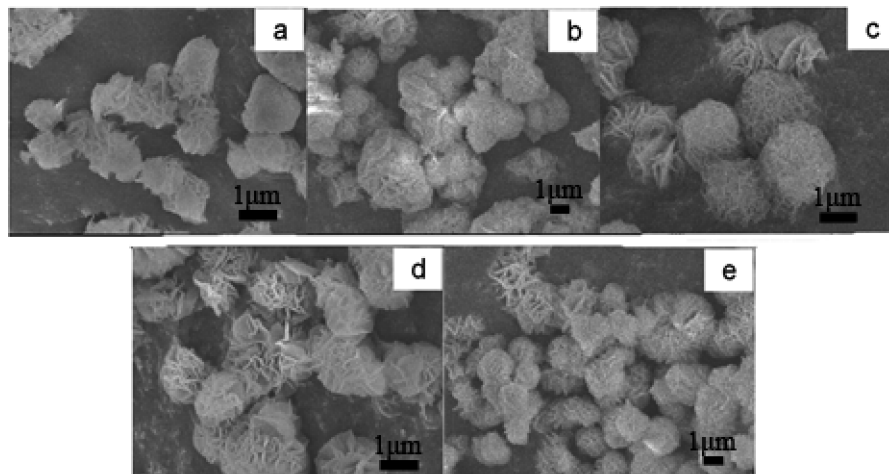


Figure 4. SEM images for the sample obtained at the synthetic time of (a) 0.5, (b) 1, (c) 2, (d) 4, and (e) 8 h.

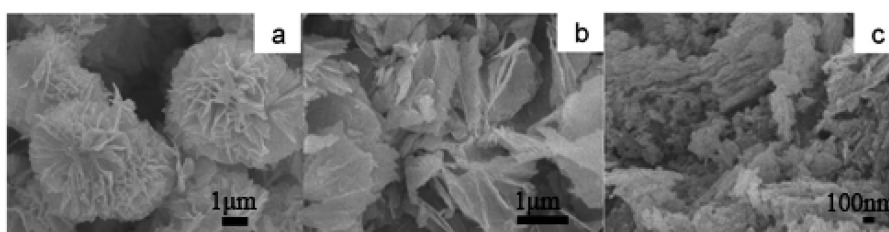


Figure 5. SEM images of the samples calcined at temperatures of (a) 300, (b) 400, and (c) 600 °C.

solution may attach to the $\text{Ni}_2\text{CO}_3(\text{OH})_2$ nucleus on the coordination sites, and the cluster gathers into colloidal spherical aggregates to minimize the surface area and decrease the energy. By random Brownian-motion-driven particle collision, the spherical aggregates may further coagulate to form multimers.⁴⁷ Due to a supersaturated $\text{Ni}_2\text{CO}_3(\text{OH})_2$ solution in their surroundings, the crystal growth is initiated preferentially from the most thermodynamically active clusters on the surface of the multimers.^{48,49} The above surfactant molecules can cap on the crystal surface selectively and lead to a limited growing direction. The $\text{Ni}_2\text{CO}_3(\text{OH})_2$ nanosheets grow along the $(\bar{1}21)$ and (002) crystallographic directions and is enclosed by $(\bar{2}01)$ facets, i.e., the widest facets, as suggested in the XRD measurement (Figure S2, Supporting Information). By means

of the Ostwald ripening process, the exterior of the multimers forms nanosheets by self-assembly along $(\bar{1}21)$ and (002) directions. As a result, the multimers are constructed into ordered nanosheet-based 3D microspheres. By means of calcination at 300 °C, the precursors are decomposed and NiO microspheres form along (200) and (220) facet directions. The whole formation process of NiO microspheres is illustrated in Figure 7. It is especially important to point out that there are two key steps to form nanosheet-based 3D microspheres: first, surfactant molecules cap on the crystal surface selectively and limit the growing direction of the crystal; second, the Ostwald ripening process ensures the formation of the microspheres with narrowly distributed diameters.

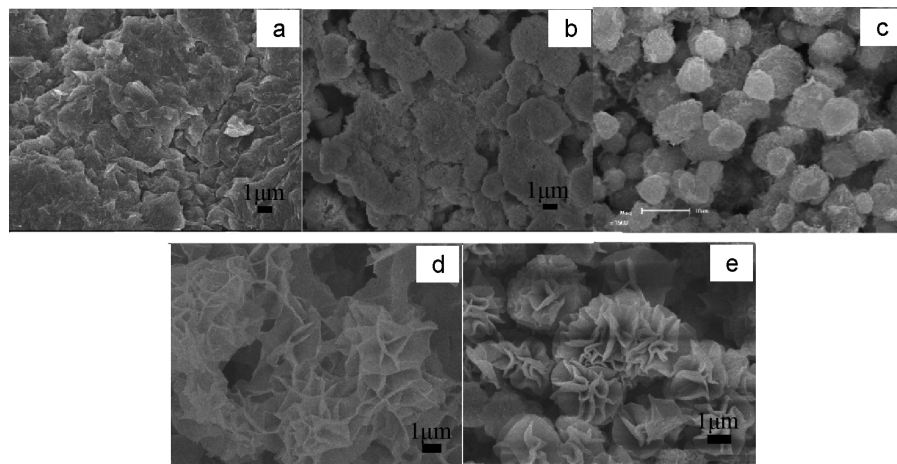


Figure 6. SEM images of the samples obtained at different synthetic conditions: (a) *n*-octanol as solvent, (b) Span80 as templates, (c) free surfactant, (d) only water as solvent and in the absence of SDS, and (e) only water as solvent and in the presence of SDS.

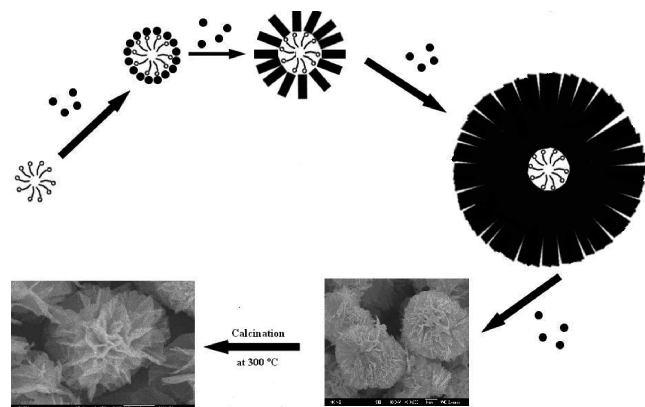


Figure 7. Whole formation process of NiO microspheres.

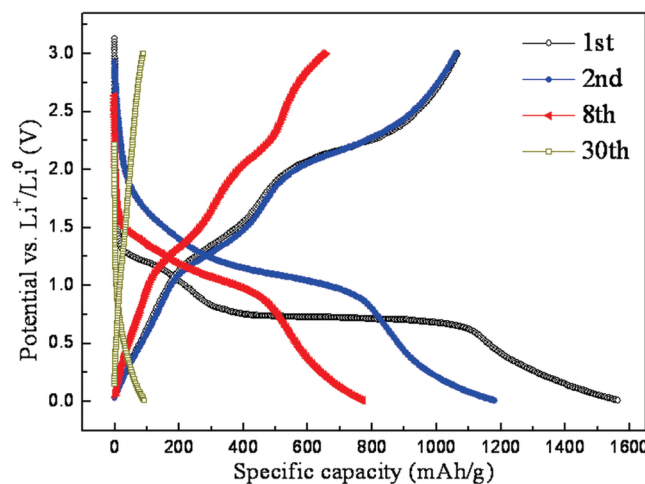


Figure 8. Charge-discharge curves of NiO microspheres tested at the current density of 50 mA/g in the potential range of 0.01–3.0 V.

3.3. Electrochemical Li Storage Performances of NiO Microspheres. The galvanostatic charge/discharge performances of NiO microspheres are shown in Figure 8. The charge/discharge capacities shown in the figures all excluded the contribution from acetylene black added in the anodes. During the first discharge, the initial discharge capacity for NiO microspheres is ~1570 mA h/g. At the same time, the voltage decreases steeply from 3.1 to 1.3 V, and then a plateau region appears at 0.7 V until a capacity of 1120 mA h/g is reached.

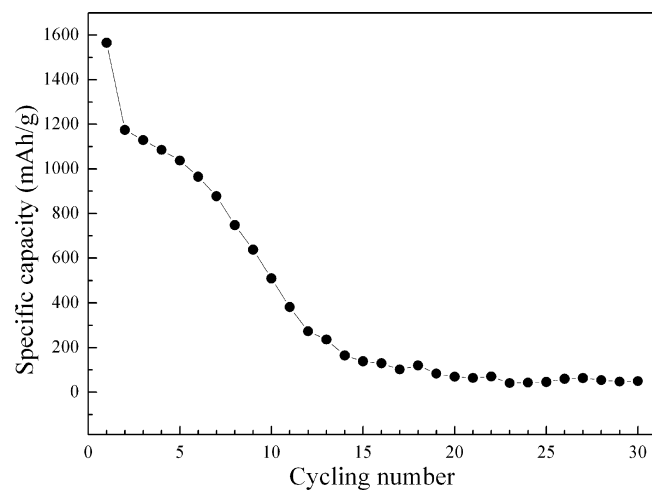


Figure 9. Cyclic performance of NiO microspheres tested at 50 mA/g in the potential range of 0.01–3.0 V.

This corresponds to a consumption of 3.12 Li's per NiO. Another slope is observed at 0.65 V, with a total first discharge capacity of 1570 mA h/g, corresponding to a consumption of 4.37 Li's per NiO. According to the mechanism in the Introduction, the discharge process should consume 2.0 Li's per NiO, but the experimental value of NiO microspheres is 4.37 Li's. The capacity of the initial discharge process may be attributed to both the formation of solid electrolyte interface (SEI) film and the polymeric gel-type layer on the surface of the material resulting from the solvent decomposition of the electrolyte.^{32,34,50,52} The irreversible capacity loss during the first discharge and charge cycle is ~500 mA h/g. In general, the irreversible capacity loss during the first cycle can be attributed to the incomplete decomposition of SEI film and Li₂O. Also, other factors, such as the intrinsic nature of the material with specific morphology, are also apparent.^{34,51–55}

However, as shown in Figure 8 and also in Figure 9, the discharge capacity degradation does not stop in the subsequent cycles. The discharge capacity before the eighth cycle is always higher than that of the theoretical capacity (718 mA h/g), due to the specific nanostructures of NiO and probably some unknown side reactions. After that, the capacity decreases sharply to a neglectable level. The severe capacity degradation and poor cycling performance should be attributed to the large volume expansion/constriction leading to the pulverization and degradation of the electrode. The volume expansion/constriction

also leads to the repeated destroy and formation of SEI film and accordingly the continuous consumption of the electrolyte. As mentioned above, the conversion (not intercalation or insertion) mechanism of transition metal oxides provides more gravimetric/volumetric capacity than graphite, but this process strongly suffers from kinetic issues which have still not been overcome to date.^{56,57} The kinetic problem of the conversion reaction lies in the lack of anionic mobility in the structure instead of electronic conduction problems. Thus, the lack of cycling performance may also result from this issue, similar to alloy reactions in Si or Sn with Li⁺. Therefore, it cannot improve the cyclic performances of oxide anode materials by preparing nanoparticles, and efforts are still necessary to modify the oxide particle/electrolyte interface and optimize the electrolyte composition.

4. Conclusion

The precursor microspheres grew directly from 2D nanosheets through a one-step solvothermal route under controlled conditions. During this procedure the decomposition of hexamethylenetetramine at temperatures ≥ 120 °C provided OH⁻ at the rate of good diffusion, and surfactants were used as templates to provide growth sites and control the growth direction of the crystals. After precursor microspheres with narrowly distributed diameters formed through the Ostwald ripening process, we could finally obtain NiO microspheres with further calcination. The unique nanostructure makes the NiO microspheres present superior Li storage performances at initial charge/discharge cycles, and further improvement in cyclic stability is still needed.

Acknowledgment. This work was supported by the 973 Program (Grant 2009CB220100) and the China-U.S. Center for Environmental Remediation and Sustainable Development in China.

Supporting Information Available: XPS spectra of NiO and XRD pattern of NiO precursor. This material is available free of charge via the Internet at <http://pubs.acs.org>.

References and Notes

- (1) Ozi, G. A. *Acc. Chem. Res.* **1997**, *30*, 17.
- (2) Caruso, F.; Caruso, R. A.; Möhwald, H. *Science* **1998**, *282*, 1111.
- (3) Mann, S. *Angew. Chem., Int. Ed.* **2000**, *39*, 3392.
- (4) Abello, S.; Medina, F.; Tichit, D.; Erez-Ramirez, P. J.; Cesteros, Y.; Salagre, P.; Sueiras, J. E. *Chem. Commun. (Cambridge)* **2005**, 1453.
- (5) Hou, Y.; Kondoh, H.; Ohta, T. *Chem. Mater.* **2005**, *17*, 3994.
- (6) Kale, B. B.; Baeg, J. O.; Lee, S. M.; Chang, H.; Moon, S. J.; Lee, C. W. *Adv. Funct. Mater.* **2006**, *16*, 1349.
- (7) Cao, A. M.; Hu, J. S.; Liang, H. P.; Wan, L. J. *Angew. Chem., Int. Ed.* **2005**, *44*, 4391. Sun, X. M.; Liu, J. F.; Li, Y. D. *Chem.—Eur. J.* **2006**, *12*, 2039.
- (8) Zhong, L. S.; Hu, J. S.; Liang, H. P.; Cao, A. M.; Song, W. G.; Wan, L. J. *Adv. Mater.* **2006**, *18*, 2426.
- (9) Chen, C. H.; Abbas, S. F.; Morey, A.; Sithambaram, S.; Xu, L. P.; Garces, H. F.; Hines, W. A.; Suib, S. L. *Adv. Mater.* **2008**, *20*, 1205.
- (10) Zhou, Y.; Antonietti, M. *J. Am. Chem. Soc.* **2003**, *125*, 14960.
- (11) Yang, H. G.; Zeng, H. C. *J. Phys. Chem. B* **2004**, *108*, 3492.
- (12) Liu, B.; Zeng, H. C. *J. Am. Chem. Soc.* **2004**, *126*, 8124.
- (13) Chang, Y.; Teo, J. J.; Zeng, H. C. *Langmuir* **2005**, *21*, 1074.
- (14) Liu, B.; Zeng, H. C. *J. Am. Chem. Soc.* **2004**, *126*, 16744.
- (15) Yao, K. X.; Zeng, H. C. *J. Phys. Chem. B* **2006**, *110*, 14736.
- (16) Li, Z.; Ding, Y.; Xiong, Y.; Yang, Q.; Xie, Y. *Chem. Commun. (Cambridge)* **2005**, 918.
- (17) O'Dwyer, C.; Navas, D.; Lavayen, V.; Benavente, E.; SantaAna, M. A.; Gonzalez, G.; Newcomb, S. B.; Sotomayor Torres, C. M. *Chem. Mater.* **2006**, *18*, 3016.
- (18) Liu, B.; Zeng, H. C. *Small* **2005**, *1*, 566.
- (19) Adler, D.; Feinleib, J. J. *Phys. Rev. B* **1970**, *2*, 3112.
- (20) Sheela, B.; Gomathi, H.; Prabhakara, R. G. *J. Electroanal. Chem.* **1995**, *394*, 267.
- (21) Miller, E. L.; Rocheleau, R. E. *J. Electrochem. Soc.* **1997**, *144*, 3072.
- (22) Makkus, R. C.; Hemmes, K.; Wir, J. H. W. D. *J. Electrochem. Soc.* **1994**, *141*, 3429.
- (23) Alcock, C. B.; Li, B. Z.; Fergus, J. W.; Wang, L. *Solid State Ionics* **1992**, *53*, 39.
- (24) Sietsma, J. R. A.; Meeldijk, J. D.; Breejen, J. P. D.; Helder, M. V.; Dillen, A. J. V.; Jongh, P. E. D.; Jong, K. P. D. *Angew. Chem., Int. Ed.* **2007**, *46*, 4547.
- (25) Lin, Y.; Xie, T.; Cheng, B. C.; Geng, B.; Zhang, L. *Chem. Phys. Lett.* **2003**, *380*, 521.
- (26) Wang, W.; Liu, Y.; Xu, C.; Zheng, C.; Wang, G. *Chem. Phys. Lett.* **2002**, *362*, 119.
- (27) Liang, Z. H.; Zhu, Y. J.; Hu, X. L. *J. Phys. Chem. B* **2004**, *108*, 3488.
- (28) Liu, X.; Qiu, G.; Wang, Z.; Li, X. *Nanotechnology* **2005**, *16*, 1400.
- (29) Wang, Y.; Zhu, Q.; Zhang, H. *Chem. Commun. (Cambridge)* **2005**, 5231.
- (30) Jiao, F.; Hill, A. H.; Harrison, A.; Berko, A.; Chadwick, A. V.; Bruce, P. G. *J. Am. Chem. Soc.* **2008**, *130*, 5262.
- (31) Wang, X.; Yu, L. J.; Hu, P.; Yuan, F. L. *Cryst. Growth Des.* **2007**, *7*, 2415.
- (32) Poizot, P.; Laruelle, S.; Gruegeon, S.; Dupont, L.; Tarascon, J. M. *Nature* **2000**, *407*, 496.
- (33) Huang, X. H.; Tu, J. P.; Zhang, C. Q.; Xiang, J. Y. *Electrochem. Commun.* **2007**, *9*, 1180.
- (34) Reddy, M. V.; Yu, T.; Sow, C.-H.; Shen, Z. X.; Lim, C. T.; Subba Rao, G. V.; Chowdari, B. V. R. *Adv. Funct. Mater.* **2007**, *17*, 2792.
- (35) Li, W.-Y.; Xu, L.-N.; Chen, J. *Adv. Funct. Mater.* **2005**, *15*, 851.
- (36) Gao, X. P.; Bao, J. L.; Pan, G. L.; Zhu, H. Y.; Huang, P. X.; Wu, F.; Song, D. Y. *J. Phys. Chem. B* **2004**, *108*, 5547.
- (37) Yuan, L.; Guo, Z. P.; Konstantinov, K.; Munroe, P.; Liu, H. K. *Electrochem. Solid-State Lett.* **2006**, *9*, A524.
- (38) Varghese, B.; Reddy, M. V.; Zhu, Y. W.; Chang, S. L.; Hoong, T. C.; Subba Rao, G. V.; Chowdari, B. V. R.; Wee, A. T. S.; Lim, C. T.; Sow, C. H. *Chem. Mater.* **2008**, *20*, 3360.
- (39) Wang, X.; Li, L.; Zhang, Y. G.; Wang, S. T.; Zhang, Z. D.; Fei, L. F.; Qian, Y. T. *Cryst. Growth Des.* **2006**, *6*, 2163. Liu, L.; Liu, H. J.; Kou, H. Z.; Wang, Y. Q.; Ren, M. M.; Zhou, Z.; Ge, M.; He, X. W. *Cryst. Growth Des.* **2009**, *9*, 113.
- (40) Liu, L.; Kou, H. Z.; Mo, W. L.; Liu, H. J.; Wang, Y. Q. *J. Phys. Chem. B* **2006**, *110*, 15218.
- (41) Liu, L.; Zhao, Y. P.; Liu, H. J.; Kou, H. Z.; Wang, Y. Q. *Nanotechnology* **2006**, *17*, 5046.
- (42) Liu, L.; Ge, M.; Liu, H. J.; Guo, C. S.; Wang, Y. Q.; Zhou, Z. *Colloids Surf., A* **2009**, *348*, 124.
- (43) Liu, L.; Liu, H. J.; Kou, H. Z.; Wang, Y. Q.; Ren, M. M.; Zhou, Z.; Ge, M.; He, X. W. *Cryst. Growth Des.* **2009**, *9*, 113.
- (44) Si, R.; Zhang, Y. W.; You, L. P.; Yan, C. H. *Angew. Chem., Int. Ed.* **2005**, *44*, 3256.
- (45) Yu, S. H.; Shu, L.; Yang, J.; Han, Z. H.; Qian, Y. T.; Zhang, Y. H. *J. Mater. Res.* **1999**, *14*, 4157.
- (46) Zhou, Y.; Antonietti, M. *J. Am. Chem. Soc.* **2003**, *125*, 14960.
- (47) Yang, H. G.; Zeng, H. C. *J. Phys. Chem. B* **2004**, *108*, 3492.
- (48) Kim, W. T.; Kim, C. D. *J. Appl. Phys.* **1986**, *60*, 2631.
- (49) Mo, M. S.; Yu, J. C.; Zhang, L. Z.; Li, S.-K. A. *Adv. Mater.* **2005**, *17*, 756.
- (50) Poizot, P.; Laruelle, S.; Gruegeon, S.; Tarascon, J. M. *J. Electrochem. Soc.* **2002**, *149*, A1212.
- (51) Gruegeon, S.; Laruelle, S.; Urbina, R. H.; Dupont, L.; Poizot, P.; Tarascon, J. M. *J. Electrochem. Soc.* **2001**, *148*, A285.
- (52) Reddy, M. V.; Madhavi, S.; Subba Rao, G. V.; Chowdari, B. V. R. *J. Power Sources* **2006**, *162*, 1312.
- (53) Reddy, M. V.; Pecquenard, B.; Vinatier, P.; Levasseur, A. *Electrochim. Commun.* **2007**, *9*, 409.
- (54) Huang, X. H.; Tu, P. J.; Zhang, B.; Zhang, C. Q.; Li, Y.; Yuan, Y. F.; Wu, H. M. *J. Power Sources* **2006**, *161*, 541.
- (55) Yuan, J. L.; Gao, Z. P.; Konstantinov, K.; Munroe, P.; Liu, H. K. *Electrochem. Solid-State Lett.* **2006**, *9*, A524.
- (56) Sauvage, F.; Tarascon, J.-M.; Baudrin, E. *J. Phys. Chem. C* **2007**, *111*, 9624.
- (57) Armand, M.; Tarascon, J.-M. *Nature* **2008**, *451*, 652.